Nanoscale Advances

ROYAL SOCIETY OF CHEMISTRY

PAPER

View Article Online
View Journal | View Issue

Cite this: *Nanoscale Adv.*, 2025, **7**, 7519

Bismuth selenide nanoflowers for internal irradiation combined with photothermal therapy for tumor sensitization and killing

Jiage Gong,†[a] Qi Wang,†[b] Ruoqi Wang,†[a] Jianhua Chen,[a] Jie Gao,[a] Jiangfeng Du *[bcd] and Jianguo Li*[ab]

The radioisotope ^{177}Lu has shown great potential in the treatment of tumors. However, free radioisotopes may cause toxicity to normal tissues and organs. Therefore, it is crucial for enhanced tumor therapy that ^{177}Lu can be retained in tumor tissues by the development of novel delivery systems. However, the efficacy of internal radiotherapy (IRT) is limited by the hypoxic microenvironment induced by the insufficient blood supply in solid tumors. Herein, we synthesized novel ^{177}Lu-labeled bismuth selenide nanoflowers that possess the peculiarity of photothermal conversion and can achieve photothermal therapy (PTT) for tumors under light conditions. Moreover, the amino group of selenocysteine in the outer layer of Bi_2Se_3 can efficiently form covalent bonds with ^{177}Lu, decreasing the side effects of free radioisotopes on normal tissues. These results demonstrate that selenocysteine-modified Bi_2Se_3 nanoflowers (Bi_2Se_3@Sec NFs) have the potential for application as radionuclide delivery carriers and radionuclide-photothermal therapy drugs.

Received 24th March 2025
Accepted 22nd August 2025

DOI: 10.1039/d5na00270b

rsc.li/nanoscale-advances

1. Introduction

Radiotherapy is a cornerstone of solid tumor treatment and includes internal radiotherapy and external radiotherapy.[1,2] In order to improve radiation sensitization, other treatments, such as surgery[3] and chemotherapy,[4] photothermal therapy,[5] and photodynamic therapy,[6–9] need to be combined. One of the main factors limiting the therapeutic effect of radiotherapy is related to the hypoxic tumor microenvironment.[10,11] If there is sufficient oxygen in tumor tissues, the efficacy of radiotherapy will be improved by enhancing radiation-induced DNA damage.[12] In the past decade, different types of multi-functional nanomaterials were synthesized, which could not only physically sensitize tumors to radiation, but also increase the blood flow in the tumor area through the photothermal conversion effect to reverse the defect of the hypoxic tumor microenvironment.[13–15] Our previous study has found that external radiation combined with photothermal therapy could enhance the sensitivity towards tumor cells,[16] but the skin radiation side effect caused by external radiation is still unavoidable.[17] However, isotope therapy, which has a short β-radiation distance (about 2.5 mm), could effectively avoid radiation damage to adjacent normal tissues during radiotherapy.[18] However, how to accurately deliver radioisotopes to tumor tissues remains a challenge.[14]

Traditional radioisotopes are connected to targeted peptides through a linker and then injected intravenously for tumor diagnosis and treatment.[19] However, the inevitable off-target effect and poor tumor tissue enrichment efficiency of the isotopes still hinder the clinical application of radioisotope therapy.[20,21] The development of nano-delivery carriers provides a new strategy for isotope delivery.[22] It has been reported that nanomaterials could be used to accurately deliver chemotherapy drugs, genes, small molecule inhibitors, and radioisotopes to the tumor site.[23,24] Pei Pei *et al.* constructed an inactivated bacterial vector with ^{125}I/^{131}I labeling (^{125}I-VNP/^{131}I-VNP) that could retain radioiodine at the tumor site for a long time and deliver it into tumor cells and tumor-associated macrophages (TAMs), thus achieving efficient internal radioisotope therapy.[25] Yueping Li *et al.* demonstrated an ^{177}Lu-labeled bioorthogonal nanoprobe for improved MR imaging, differentiating, and downstaging of bladder tumors.[26] Xi-Yang Cui *et al.* installed a sulfur(VI) fluoride exchange (SuFEx) chemistry-based linker on radiopharmaceuticals to prevent excessively fast tumor clearance.[20] Moreover, nano-drugs can be maximally enriched in the tumor site by intratumoral injection.

[a]*National Atomic Energy Agency Nuclear Technology (Nonclinical Evaluation of Radiopharmaceuticals) Research and Development Center, CNNC Key Laboratory on Radiotoxicology and Radiopharmaceutical Preclinical Evaluation, China Institute for Radiation Protection, Taiyuan 030001, China. E-mail: ljg2547@163.com*

[b]*College of Pharmacy, Shanxi Medical University, Jinzhong, 030619, Shanxi Province, China. E-mail: dujf@sxmu.edu.cn*

[c]*Department of Medical Imaging, Shanxi Key Laboratory of Intelligent Imaging and Nanomedicine, First Hospital of Shanxi Medical University, Taiyuan, 030001, Shanxi Province, China*

[d]*Collaborative Innovation Center for Molecular Imaging of Precision Medicine, Shanxi Medical University, Taiyuan 030001, Shanxi Province, China*

† These authors contributed equally to this work.

Therefore, the toxic side effects of free radioisotopes on normal tissues could be effectively avoided when the radioisotopes are delivered by nanocarriers and administered by intratumoral injection.

Based on our previous study, the biodegradable selenocysteine-based bismuth selenide nanoflowers (Bi_2Se_3@Sec NFs) exhibited excellent biosafety.[27] Herein, the amino group of selenocysteine has been found to covalently bind with ^{177}Lu ($t_{1/2}$ = 6.65 days). Moreover, the photothermal conversion effect of Bi_2Se_3@Sec NFs could increase the temperature of the tumor area. After the intratumoral injection of ^{177}Lu-labeled Bi_2Se_3@Sec NFs, the β-rays emitted by ^{177}Lu could continuously kill tumor cells by the long-term retention effect of nanomaterials in the tumor tissues. At the same time, the γ-rays emitted by ^{177}Lu could also be used for single-photon emission computed tomography (SPECT) imaging of the tumors. This novel study provides a new idea for the precise delivery of ionic isotopes to tumor tissues (Scheme 1).

2. Experimental

Material

The ^{177}Lu isotope was purchased from the China Institute of Atomic Energy. L-Selenocysteine was purchased from J&K Scientific. Bismuth nitrate pentahydrate ($Bi(NO_3)_3\cdot 5H_2O$) was purchased from Beijing Chemical Works. HT-29 cells were purchased from Wuhan Pricella Biotechnology Co., Ltd. RPMI Medium 1640 was purchased from Gibco (USA). Every Green Fetal bovine serum was purchased from Tianhang Biotechnology Co., LTD. Penicillin-streptomycin was purchased from SEVEN (Beijing) Biotechnology Co., LTD. PBS, trypsin, Cell Counting Kit-8, Giemsa stain, and polyformaldehyde fixative were purchased from Solarbio Life Sciences.

Synthesis

L-Selenocysteine aqueous solution, sodium hydroxide aqueous solution, and deionized water were added sequentially to a three-necked flask and thoroughly mixed by sonication. The mixture was then heated to 80 °C. Subsequently, a $Bi(NO_3)_3\cdot 5H_2O$ ethylene glycol solution was rapidly injected into a sealed flask, and the reaction was continued for 3 h at 80 °C. After cooling to room temperature, the products were collected by centrifugation and washed three times to obtain Bi_2Se_3@Sec NFs.

To perform ^{177}Lu labelling, 300 μCi of ^{177}Lu ($^{177}LuCl_3$) was mixed with Bi_2Se_3@Sec NFs solution (water, 500 μg mL^{-1}) and the mixture was stirred (500 rpm) at room temperature for 24 h. ^{177}Lu-labelled Bi_2Se_3@Sec NFs were then obtained by centrifugation at 8000 rpm for 30 minutes at 4 °C. Subsequently, the labelling rate and radiolabelling stability were determined.

Characterization

A scanning electron microscope was employed to characterize the morphology and size of the nanoflowers. Energy dispersive X-ray spectroscopy and X-ray photoelectron spectroscopy were used to analyze the chemical composition of nanomaterials.

Investigation of the photothermal properties of the nanoflowers

Different concentrations of Bi_2Se_3@Sec NFs solution (50, 100, 200, 400, 600, 800, and 1000 μg mL^{-1}) were prepared; 1 mL of each solution was placed in a cuvette and irradiated by a laser

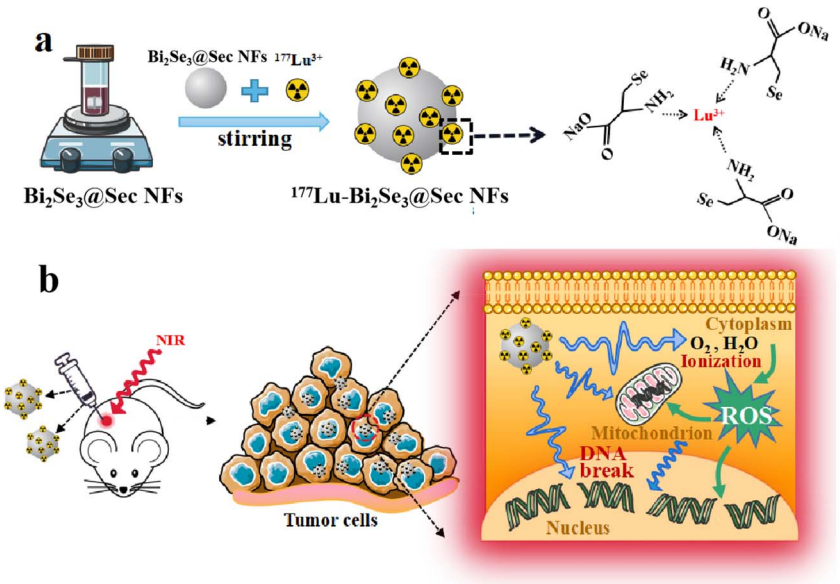

Scheme 1 Schematic of the synthesis of the Bi_2Se_3@Sec nanoflower-labeled radionuclide ^{177}Lu (a). The therapeutic strategy for ^{177}Lu–Bi_2Se_3@Sec NFs combined with photothermal therapy for improving efficacy in the tumor and simultaneously reducing side effects in normal tissues (b).

(808 nm, power 1.0 W cm^{-2}) for 10 minutes. The temperature of the solution was monitored using a thermal infrared imaging camera (Fluke Ti480U). The temperature changes of the samples were recorded every 30 s, and the temperature was plotted against time.

Next, 1 mL of Bi_2Se_3@Sec NFs solution (500 μg mL^{-1}) was placed in a cuvette and irradiated by a laser (808 nm, power 1.0 W cm^{-2}) for 10 minutes, with an interval of 10 min; this was repeated four times. The temperature of the solution was monitored using a thermal infrared imaging camera (Fluke Ti480U). The temperature changes of the samples were recorded every 30 s, and the temperature was plotted against time. An equal volume of deionized water was used as a control under the same experimental conditions.

Then, 1 mL of Bi_2Se_3@Sec NFs solution (500 μg mL^{-1}) was placed in a cuvette and the laser (808 nm, the power was set to 0.5, 1.0, and 1.5 W cm^{-2}, respectively) was used to irradiate the sample for 10 minutes. After cooling to the initial temperature, the temperature of the solution was monitored using a thermal infrared imaging camera. The temperature changes of the samples were recorded every 30 s. An equal volume of deionized water was used as a control under the same experimental conditions.

Cell culture

Cells were cultured in a cell incubator containing 5% CO_2 at 37 °C and cultured in RPMI Medium 1640 with 10% (v/v) FBS and 1% (v/v) penicillin/streptomycin. Cells were passaged at 1 day intervals.

Cell survival assay

The relative cell viabilities were evaluated by CCK-8 assay. HT-29 cells were inoculated into 96-well plates at 1×10^4 cells per well. After 24 h of culturing, the old medium was discarded, and different concentrations of Bi_2Se_3@Sec NFs (0, 5, 10, 20, 40, 60, 80, 100 μg mL^{-1}) were added and incubated for 24 h. The old medium was discarded, and fresh complete medium containing 10 μL CCK-8 was added to each well. After 2 h of incubation, the absorbance value at 450 nm was measured by a microplate reader (Multiskan GO), and then the cell survival rate of different concentration groups was calculated.

Cellular uptake assay

HT-29 cells were inoculated into 6-well plates and treated with PBS, $^{177}LuCl_3$ (50 μCi), Bi_2Se_3@Sec NFs (25 μg mL^{-1}), and ^{177}Lu–Bi_2Se_3@Sec NFs (50 μCi, 25 μg mL^{-1}) 24 h later. After incubation for 1, 4, 12, and 24 h, respectively, the cells were rinsed 2–3 times with PBS, then digested and collected in a centrifuge tube. Finally, the radioactivity of the cells was detected by a gamma counter (WIZARD 2480), and the cell uptake rate was calculated.

The clonogenic assay

HT-29 cells were inoculated into a 6-well plate at 2000 cells per well, and treated with the following treatments 24 h later: ①PBS; ②Bi_2Se_3@Sec NFs (25 μg mL^{-1}); ③$^{177}LuCl_3$ (50 μCi); ④^{177}Lu–Bi_2Se_3@Sec NFs (50 μCi, 25 μg mL^{-1}). After 24 h, the cells were replaced with fresh complete medium and incubated for 10 to 15 days, with the medium changed every 2 to 3 days. When the clones grew to an appropriate size (colonies of about 50 cells), they were fixed with methanol, stained with 10% Giemsa staining solution, washed, dried, and photographed. Finally, the number of clones was counted, the clone formation rate of cells was calculated, and the therapeutic effect was compared.

DNA double-strand break detection

The DNA double-strand break (DSB) levels were detected by immunofluorescence analysis. HT-29 cells were inoculated on coverslips, and different treatments (① PBS; ② near-infrared radiation (NIR, 1.0 W cm^{-2}, 808 nm); ③ $^{177}LuCl_3$ (50 μCi); ④ ^{177}Lu–Bi_2Se_3@Sec NFs + NIR (50 μCi, 25 μg mL^{-1})) were performed after 24 hours of culturing. After incubating the above medium for 24 hours, near-infrared radiation (NIR) was applied. Firstly, 4% paraformaldehyde and 0.3% Triton X-100-PBS buffer were employed to fix and perforate cells. Then, 5% bovine serum albumin (BSA) was added for 1 hour at room temperature. Next, the cells were incubated with antibodies against γ-H2AX overnight at 4 °C and Cy3-labeled anti-rabbit lgG for 2 hours at room temperature, sequentially. Finally, the nuclei were stained with DAPI and sealed with 10% glycerol. Fluorescence images were captured using a Nikon Ti-A1 laser confocal microscope. Representative images are shown.

Animals

All animal procedures were performed in accordance with the Guidelines for Care and Use of Laboratory Animals of the China Institute for Radiation Protection and approved by the Animal Ethics Committee of the China Institute for Radiation Protection (CIRP-IACUC-(G)2023331). Female experimental animals, aged 7–8 weeks, with a specific pathogen-free (SPF) grade and an average body weight of 20 ± 2 g, were obtained from Changzhou Cavens Laboratory Animal Co., Ltd. The animals were housed in a controlled environment at a temperature of 25 °C and 50% air humidity.

Biodistribution of drugs

The HT-29 cell line was selected to establish the tumor animal model. When the subcutaneous tumor volume reached about 100 mm^3, 24 tumor-bearing mice were randomly divided into 8 groups, respectively, with 3 mice in each group: ①$^{177}LuCl_3$ (2 h), ②$^{177}LuCl_3$ (24 h), ③$^{177}LuCl_3$ (48 h), ④$^{177}LuCl_3$ (10 d), ⑤^{177}Lu–Bi_2Se_3@Sec NFs (2 h), ⑥^{177}Lu–Bi_2Se_3@Sec NFs (24 h), ⑦^{177}Lu–Bi_2Se_3@Sec NFs (48 h), ⑧^{177}Lu–Bi_2Se_3@Sec NFs (10 d). Each group of mice was injected with $^{177}LuCl_3$ and ^{177}Lu–Bi_2Se_3 NFs *via* intratumoral injection, respectively, and the radioactivity was 100 μCi. The heart, liver, spleen, lung, kidney, stomach, intestine, and tumors were taken at the corresponding time points. Subsequently, the organ radioactivity was detected by a gamma counter.

The effects of radionuclide therapy combined with photothermal therapy on tumor treatment

The HT-29 cell line was selected to establish the tumor animal model. When the subcutaneous tumor volume reached about 70 mm^3, the tumor-bearing nude mice were randomly divided into 7 groups (① Control group; ② Bi_2Se_3@Sec NFs (1.5 mg kg^{-1}); ③ NIR (1.0 W cm^{-2},808 nm); ④ $^{177}LuCl_3$(300 μCi); ⑤ ^{177}Lu–Bi_2Se_3@Sec NFs(300 μCi, 1.5 mg kg^{-1}); ⑥ Bi_2Se_3@Sec NFs + NIR (1.5 mg kg^{-1}, 1.0 W cm^{-2},808 nm); ⑦ ^{177}Lu–Bi_2Se_3@Sec NFs + NIR (300 μCi, 1.5 mg kg^{-1}, 1.0 W cm^{-2},808 nm)), with 3 mice in each group.

As shown in Fig. 2, mice in groups ② and ⑥ were injected with Bi_2Se_3@Sec NFs solution, mice in groups ⑤ and ⑦ were injected with ^{177}Lu–Bi_2Se_3@Sec NFs solution, and mice in group ④ were injected with $^{177}LuCl_3$ solution by intratumoral injection. Then, groups ③, ⑥, and ⑦ received 1 W cm^{-2}, 808 nm laser irradiation for 10 min, and the local tumor temperature changes were monitored by thermal imaging. At the end of treatment, the body weight and tumor volume of the mice were monitored every other day until day 20 after treatment. Whole blood was collected from mice by enucleation of the eyeballs, and the mice were sacrificed by cervical dislocation. The important organs of the mice (including the heart, liver, spleen, lungs, and kidneys) as well as their femur and tumors were collected and weighed to evaluate the therapeutic effect of different groups of tumors.

2. Results and discussion

Characterization and radiochemical properties of nanocarriers

In our previous report, the Bi_2Se_3@Sec nanoflowers exhibited good biosafety and microwave sensitization effects. The typical scanning electron microscopy (SEM) images shown in Fig. 1a reveal that Bi_2Se_3@Sec NFs are in the shape of flower clusters (Fig. 1a) with a diameter of about 500–1000 nm. Energy-dispersive X-ray spectroscopy (EDS) and X-ray photoelectron spectroscopy (XPS) results for Bi_2Se_3@Sec NFs further confirmed that the nanoflowers were composed of Bi and Se elements (Fig. 1b and c). The labeling yield of ^{177}Lu was 88.15% ± 1% and it showed good radiostability in PBS and serum (37 °C) (Fig. 1d). These experimental results indicate the successful synthesis and high purity of Bi_2Se_3@Sec NFs, and their isotope labeling.

Photothermal conversion effect of Bi_2Se_3@Sec NFs *in vitro*

As shown in Fig. 2a and c, under the irradiation of the 808 nm laser (power density 1.0 W cm^{-2}), the temperature of the

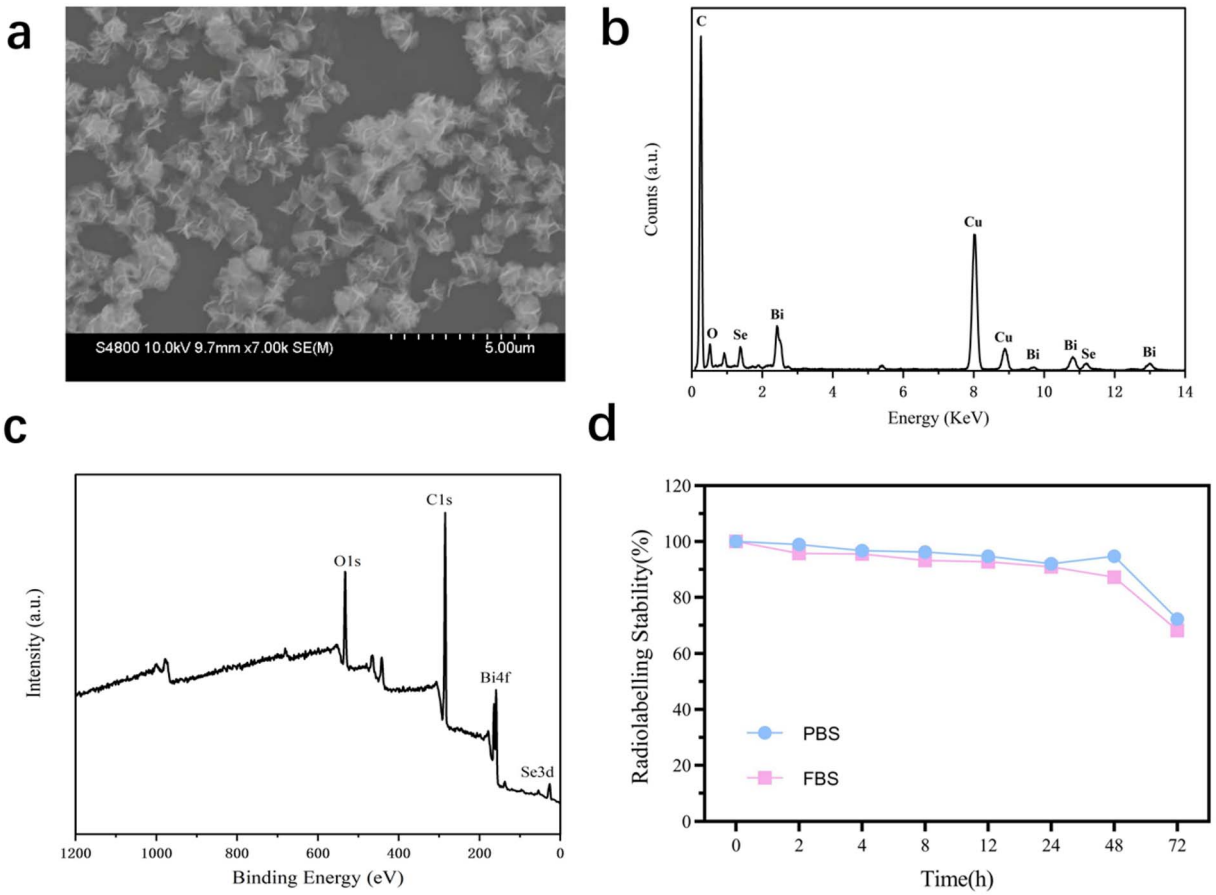

Fig. 1 (a) SEM image of Bi_2Se_3@Sec NFs (scale bar: 5 μm). (b) EDS analysis of Bi_2Se_3@Sec NFs. (c) XPS analysis of Bi_2Se_3@Sec NFs. (d) Radiological stability curves of ^{177}Lu–Bi_2Se_3@Sec NFs in PBS/FBS.

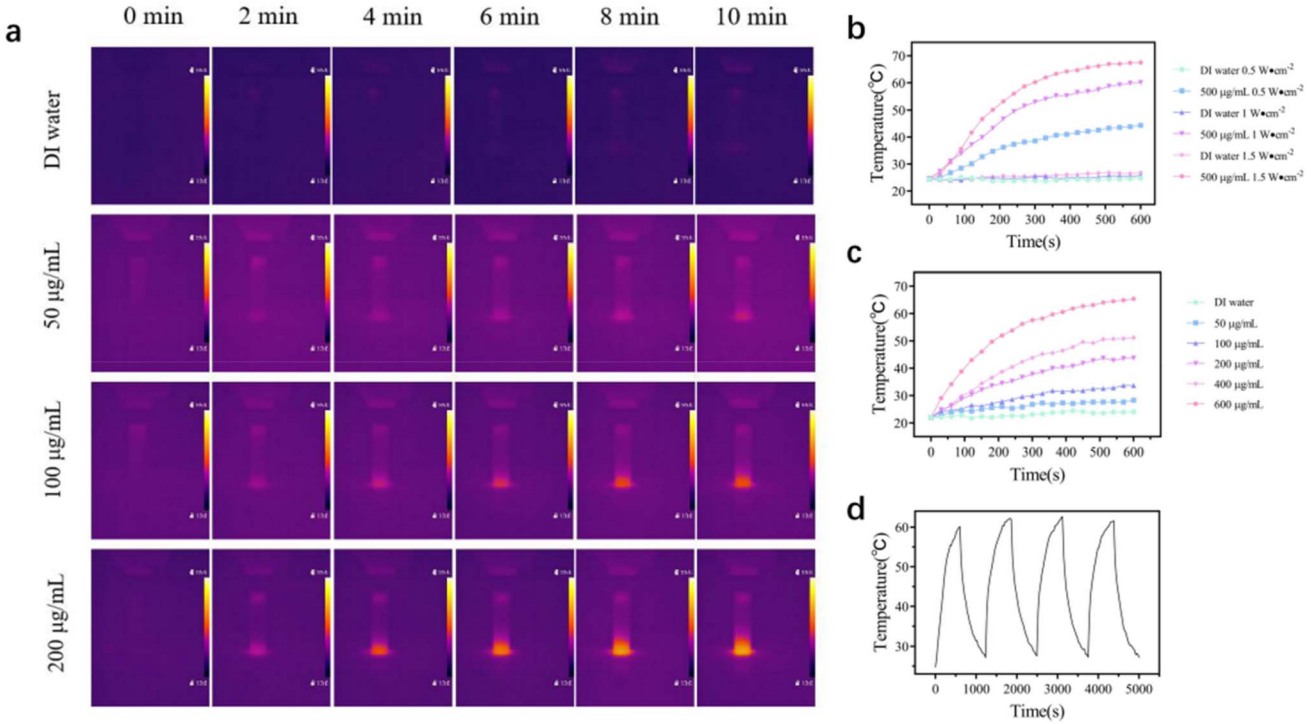

Fig. 2 (a) The infrared thermal images of Bi_2Se_3@Sec NFs with various concentrations of dH_2O at different time points under 808 nm laser irradiation (1.0 W cm^{-2}). (b) The comparison of temperature elevation between Bi_2Se_3@Sec NFs (500 μg mL^{-1}) and dH_2O under 808 nm laser irradiation at different powers. (c) The heating curves of Bi_2Se_3@Sec NFs with different concentrations under 808 nm laser irradiation (1.0 W cm^{-2}). (d) Rise and fall curves of Bi_2Se_3@Sec NFs (500 μg mL^{-1}) for five laser irradiation cycles under 808 nm laser irradiation (1.0 W cm^{-2}).

Bi_2Se_3@Sec NFs aqueous solution increased with irradiation time, while the temperature of the control group had no significant change. Under the same concentration of nanoflowers (500 μg mL^{-1}) with different laser power, the temperature of the aqueous solution of nanoflowers rose rapidly with the increase of laser power, while the temperature of the aqueous solution in the control group did not change significantly (Fig. 2b). Bi_2Se_3@Sec NFs nanoflowers (600 μg mL^{-1}) increased to 65.4 °C after 10 minutes of laser (1.0 W cm^{-2}) exposure, an increase of 41.4 °C from the original temperature. Further experiments showed that the photothermal conversion ability of the Bi_2Se_3@Sec NFs aqueous solution did not decrease after 4 cycles of continuous heating

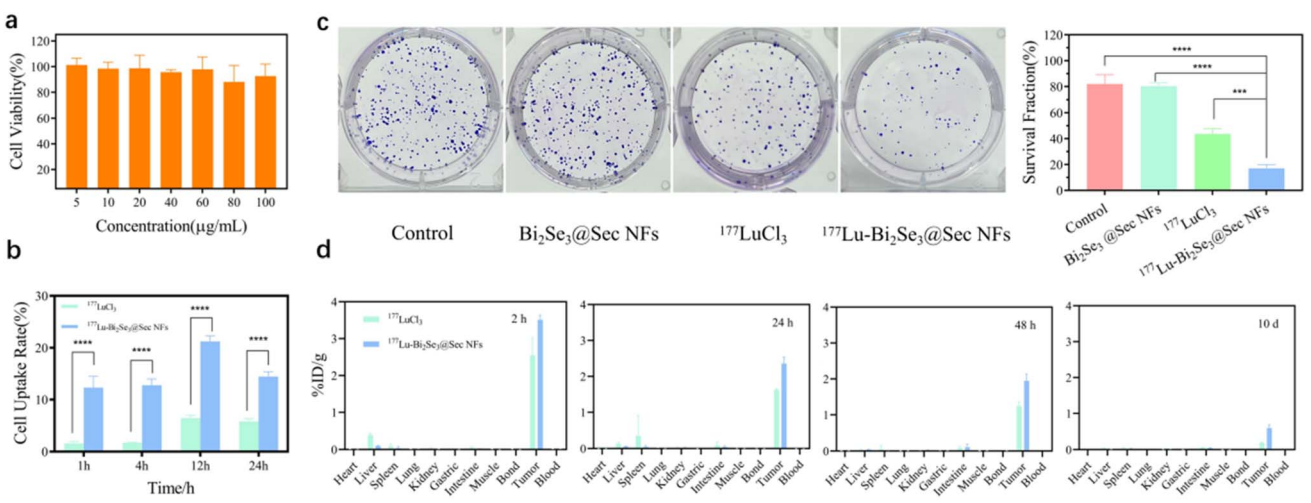

Fig. 3 (a) Cell viability of HT29 cells after treatment with Bi_2Se_3@Sec NFs. (b) *In vitro* cellular uptake of ^{177}Lu–Bi_2Se_3@Sec NFs and $^{177}LuCl_3$. (c) Cell cloning experiment of HT-29 cells after different treatments. (d) The biological distribution of free ^{177}Lu and ^{177}Lu–Bi_2Se_3@Sec NFs in mice was determined at different times after intratumoral injection.

and cooling, indicating its stable photothermal conversion performance (Fig. 2d).

Cell culture experiment

For further research, the HT-29 cells were employed to evaluate the cytotoxicity of Bi_2Se_3@Sec NFs. After incubation with different concentrations of Bi_2Se_3@Sec NFs for 24 h, the HT-29 cell viability was evaluated by CCK-8 assay. The results showed that the cell viability remained above 90% when the concentration of Bi_2Se_3@Sec NFs reached 100 μg mL^{-1}, indicating that Bi_2Se_3@Sec NFs had no obvious toxicity toward the cells (Fig. 3a). In the cell uptake experiment, the radioactivity of different groups was detected 1, 4, 12, and 24 h after treatment (Fig. 3b). The results showed that the intracellular radioactivity in the $^{177}LuCl_3$ group was significantly lower than that in the ^{177}Lu–Bi_2Se_3@Sec NFs ($p < 0.05$), indicating that ^{177}Lu–Bi_2Se_3@Sec NFs had higher cellular uptake efficiency. In the clone formation assay, there was no difference in the clone formation rate between the Bi_2Se_3@Sec NFs treatment and the control group, further indicating the good safety of Bi_2Se_3@Sec NFs at the cellular level (Fig. 3c). In contrast, the clone formation rate of $^{177}LuCl_3$ group was 53.26%, and that of ^{177}Lu–Bi_2Se_3@Sec NFs was 20.73%, which was significantly different ($p < 0.05$), indicating that ^{177}Lu–Bi_2Se_3@Sec NFs had a significant effect on inhibiting the growth of tumor cells. Confocal microscopy was used to detect γ-H2AX foci in the cell nuclei as a quantitative marker of DNA double-strand breaks (Fig. S1); prominent, higher-density γ-H2AX foci were observed in the ^{177}Lu–Bi_2Se_3@Sec NFs + NIR group when compared to the group with $^{177}LuCl_3$ or NIR alone. The density of γ-H2AX foci was the highest in the synergistic NIR+^{177}Lu–Bi_2Se_3@Sec NFs group. These results suggest that Bi_2Se_3@Sec NFs-mediated PTT/IRT combined therapy provides a means to efficiently kill cancer cells.

The organ radioactivity was measured at 2 h, 24 h, 48 h, and 10 d after intratumoral injection (Fig. 3d). The results showed that the radioactivity of ^{177}Lu–Bi_2Se_3@Sec NFs in the tumor was always at a high level, and a small amount of radioactive material accumulated in the liver and kidney. Over time, normal tissues showed little radioactivity. Compared with free ^{177}Lu, ^{177}Lu–Bi_2Se_3@Sec NFs were better retained in the tumor at different time points.

The evaluation of Bi_2Se_3@Sec NFs combined with photothermal therapy *in vivo*

Encouraged by the effects of ^{177}Lu–Bi_2Se_3@Sec NFs *in vitro*, we further investigated the therapeutic effect *in vivo* by intratumoral injection. As shown in Fig. S2 and S3, the temperature of the tumor region changed from 38.8 to 51.7 °C under the 808 nm laser (1 W cm^{-2}) irradiation for 10 min, while the control group treated with PBS had no obvious temperature increase. Compared to the control group, the inhibitory effect of the ^{177}Lu–Bi_2Se_3@Sec NFs + NIR group was better after 20 days. At the end of treatment, tumors were dissected, weighed, and photographed (Fig. 4b and d). The tumor weights and sizes were the least in the different treatment groups, which confirmed the

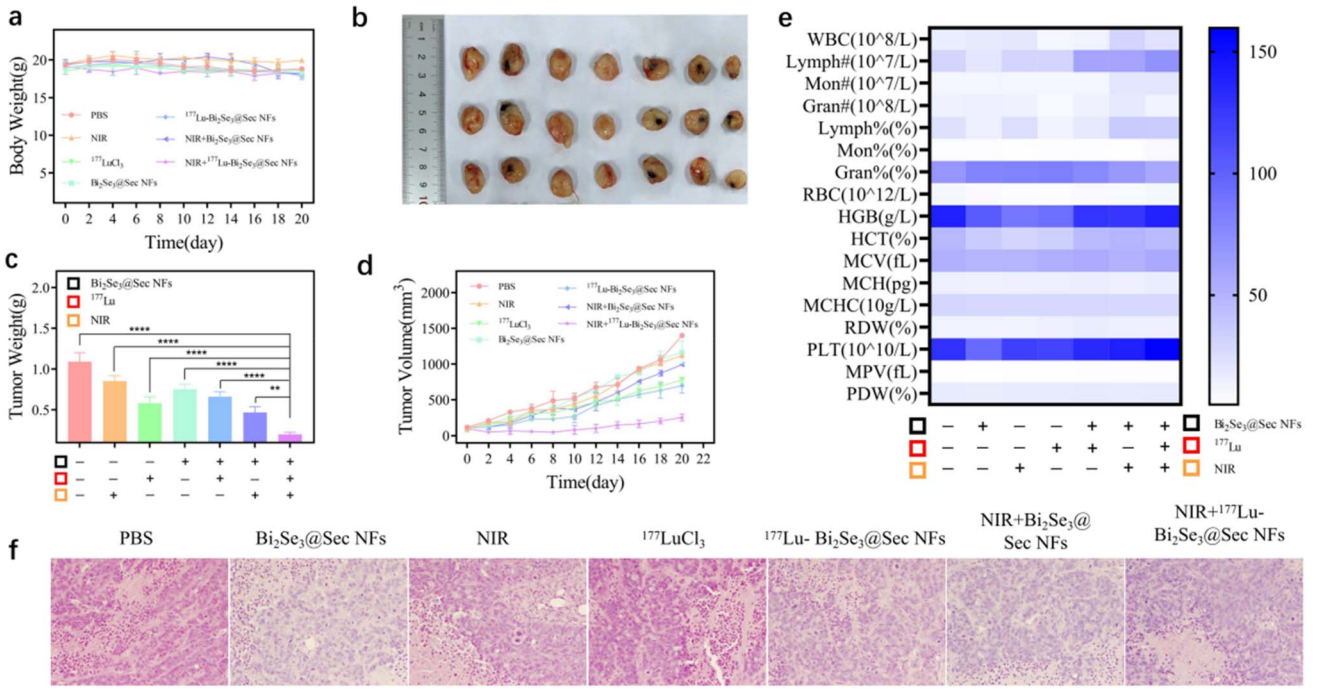

Fig. 4 (a) The body weight curves of different groups of mice during treatment time. (b) The images of isolated tumors. (c) Tumor weights in different treatment groups at the time of dissection (day 20). (d) The tumor growth curves of different groups of mice during treatment time. (e) Hematological parameters of different groups. (f) The pathological characteristics of representative tumor tissues in different groups: H&E (scale bar: 200 μm).

synergistic effect of PTT and radionuclide therapy. In the hematoxylin and eosin (HE) staining assay, the tumor tissues of the ^{177}Lu–Bi_2Se_3@Sec NFs + NIR group showed varying degrees of necrosis, vacuolar degeneration in the cytoplasm, reduced tumor cell clusters, increased intercellular space, and sparse distribution of tumor cells compared with the control group. The nuclei were variable in size and the degree of staining, and there was multifocal or flaky tumor cell necrosis. In the ^{177}Lu and PTT group, only partial regions of tumor tissue were destroyed. As shown in Fig. 4a, there was no significant change in body weight between the control group and all treatment groups during the 20 days of treatment, indicating that the nanomedicine had no significant side effects on mice. According to the results of the blood routine test, there was no significant difference in WBC, RBC, LYM, and other indices between all treatment groups and the control group, indicating that the materials and treatment methods did not cause obvious toxic side effects.

4. Conclusions

In summary, we have developed a strategy to sensitize and kill tumors by combining a ^{177}Lu-labeled nanoradioenhancer with photothermal therapy. On the one hand, Bi_2Se_3@Sec NFs have good biocompatibility and photothermal properties, and radiation stability under the radionuclide irradiation. This suggests that the Bi_2Se_3@Sec NFs can be good photothermal agents for tumor photothermal therapy. On the other hand, we stabilized Bi_2Se_3@Sec NFs with the radioactive nuclide ^{177}Lu through ion exchange reactions. The uptake of ^{177}Lu–Bi_2Se_3@Sec NFs on HT-29 cells and the retention ability in tumor tissue were all higher than those of the $^{177}LuCl_3$ group (Fig. 3b and d). In this study, Bi_2Se_3@Sec NFs-loaded ^{177}Lu combined with photothermal therapy can further improve the tumor inhibition rate compared with single treatments. With the further exploration of methods and the adjustment of the radionuclide dose, Bi_2Se_3@Sec NFs loaded with ^{177}Lu radionuclide and combined with photothermal therapy is expected to become a new method to effectively kill cancer cells and protect normal tissues and organs as much as possible.

Author contributions

J.-G. G., Q. W., R-Q. W.: Writing-original draft and investigation. J.-H. C, J. G.: Investigation and data curation. J.-F. D., J.-G. L.: Project administration, supervision, and writing review and editing.

Conflicts of interest

The authors declare that they have no known competing financial interests or personal relationships that could influence the work reported in this paper.

Data availability

The data supporting this article have been included as part of the SI. See DOI: https://doi.org/10.1039/d5na00270b.

Acknowledgements

This work was supported by the Social Development Projects of Key R&D Program in Shanxi Province (202303021221223) and CIRP Open Fund of Radiation Protection Laboratories (CIRP-CAEA20240201).

References

1 J.-F. Chatal and C. A. Hoefnagel, *Lancet*, 1999, **354**, 931–935.
2 L. Y. Gong, Y. J. Zhang, C. C. Liu, M. Z. Zhang and S. X. Han, *Int. J. Nanomed.*, 2021, **16**, 1083–1102.
3 M. C. van Maaren, L. de Munck, G. H. de Bock, J. J. Jobsen, T. van Dalen, S. C. Linn, P. Poortmans, L. J. A. Strobbe and S. Siesling, *Lancet Oncol.*, 2016, **17**, 1158–1170.
4 J. X. Dai, B. Zhang, Y. X. Su, Y. F. Pan, Z. K. Ye, R. Cai, G. J. Qin, X. Y. Kong, Y. Y. Mo, R. J. Zhang, Z. C. Liu, Y. Xie, X. L. Ruan and W. Jiang, *JAMA Oncol.*, 2024, **4**, 456–463.
5 Y. Yong, X. J. Cheng, T. Bao, M. Zu, L. Yan, W. Y. Yin, C. C. Ge, D. L. Wang, Z. J. Gu and Y. L. Zhao, *ACS Nano*, 2015, **9**, 12451–12463.
6 W. Rao, Z. S. Deng and J. Liu, *Crit. Rev. Bioeng.*, 2010, **38**, 101–116.
7 R. B. Mokhtari, T. S. Homayouni, N. Baluch, E. Morgatskaya, S. Kumar, B. Das and H. Yeger, *Oncotarget*, 2017, **8**, 38022–38043.
8 Y. W. Wang, K. Ma, M. M. Kang, D. Y. Yan, N. Niu, S. S. Yan, P. P. Sun, L. Z. Zhang, L. J. Sun, D. Wang, H. Tan and B. Z. Tang, *Chem. Soc. Rev.*, 2024, **53**, 12014–12042.
9 Y. Chao, L. G. Xu, C. Liang, L. Z. Feng, J. Xu, Z. L. Dong, L. L. Tian, X. Yi, K. Yang and Z. Liu, *Nat. Biomed. Eng.*, 2018, **2**, 611–621.
10 F. Mudassar, H. Shen, K. M. Cook and E. Hau, *J. Med. Imaging Radiat. Oncol.*, 2022, **66**, 560–574.
11 D. C. Singleton, A. Macann and W. R. Wilson, *Nat. Rev. Clin. Oncol.*, 2021, **18**, 751–772.
12 Z. Chen, F. F. Han, Y. Du, H. Q. Shi and W. C. Zhou, *Signal Transduction Targeted Ther.*, 2023, **8**, 70.
13 L. Y. Gong, Y. J. Zhang, C. C. Liu, M. Z. Zhang and S. X. Han, *Int. J. Nanomed.*, 2021, **16**, 1083–1102.
14 G. S. Song, L. Cheng, Y. Chao, K. Yang and Z. Liu, *Adv. Mater.*, 2017, **29**, 1700996.
15 M. Varzandeh, L. Sabouri, V. Mansouri, M. Gharibshahian, N. Beheshtizadeh, M. R. Hamblin and N. Rezaei, *Bioeng. Transl. Med.*, 2023, **8**, e10498.
16 J. F. Du, Z. J. Gu, L. Yan, Y. Yong, X. Yi, X. Zhang, J. Liu, R. F. Wu, C. C. Ge, C. Y. Chen and Y. L. Zhao, *Adv. Mater.*, 2017, **29**, 1701268.
17 K. Wang and J. E. Tepper, *Ca-Cancer J. Clin.*, 2021, **71**, 437–454.
18 U. Hennrich and M. Eder, *Pharmaceuticals*, 2022, **15**, 1292.

19 L. Chen, X. Y. Zhong, X. Yi, M. Huang, P. Ning, T. Liu, C. C. Ge, Z. F. Chai, Z. Liu and K. Yang, *Biomaterials*, 2015, **66**, 21–28.
20 X. Y. Cui, Z. Li, Z. Kong, Y. Liu, H. Meng, Z. H. Wen, C. L. Wang, J. Y. Chen, M. X. Chen, Y. Y. Li, J. Y. Gao, W. J. Zhu, Z. X. Hao, L. Huo, S. Y. Liu, Z. Yang and Z. B. Liu, *Nature*, 2024, **630**, 206–213.
21 E. O. Aboagye, T. D. Barwick and U. Haberkorn, *Ca-Cancer J. Clin.*, 2023, **73**, 255–274.
22 L. M. Sun, H. M. Liu, Y. Q. Ye, Y. Lei, R. Islam, S. M. Tan, R. S. Tong, Y. B. Miao and L. L. Cai, *Signal Transduction Targeted Ther.*, 2023, **8**, 418.
23 X. Z. Zhu and S. L. Li, *Mol. Cancer*, 2023, **22**, 94.
24 S. Raj, S. Khurana, R. Choudhari, K. K. Kesari, M. A. Kamal, N. Garg, J. Ruokolainen, B. C. Das and D. Kumar, *Semin. Cancer Biol.*, 2021, **69**, 166–177.
25 P. Pei, Y. Zhang, Y. C. Jiang, W. H. Shen, H. Chen, S. Yang, Y. X. Zhang, X. Yi ang and K. Yang, *ACS Nano*, 2022, **16**, 11325–11337.
26 Y. P. Li, S. S. Shan, R. R. Zhang, C. P. Sun, X. L. Hu, J. D. Fan, Y. Wang, R. X. Duan and M. Y. Gao, *ACS Nano*, 2024, **18**, 17209–17217.
27 L. Gao, H. L. Yan, S. Zhu, X. C. Wang, Y. Tan, J. F. Du, D. P. Feng, H. Zhang and Z. J. Gu, *Nano Today*, 2021, **41**, 101314.